3. Shima F, et al. (2010) Structural basis for conformational dynamics of GTP-bound Ras protein. *J Biol Chem* 285(29):22696–22705.
4. Araki M, et al. (2011) Solution structure of the state 1 conformer of GTP-bound H-Ras protein and distinct dynamic properties between the state 1 and state 2 conformers. *J Biol Chem* 286(45):39644–39653.
5. Margarit SM, et al. (2003) Structural evidence for feedback activation by Ras.GTP of the Ras-specific nucleotide exchange factor SOS. *Cell* 112(5):685–695.
6. Güntert P, Mumenthaler C, Wüthrich K (1997) Torsion angle dynamics for NMR structure calculation with the new program DYANA. *J Mol Biol* 273(1):283–298.
7. Brünger AT, et al. (1998) Crystallography & NMR system: A new software suite for macromolecular structure determination. *Acta Crystallogr D Biol Crystallogr* 54(Pt 5):905–921.
8. Hajduk PJ, Olejniczak ET, Fesik SW (1997) One-dimensional relaxation- and diffusion-edited NMR methods for screening compounds that bind to macromolecules. *J Am Chem Soc* 119:12257–12261.

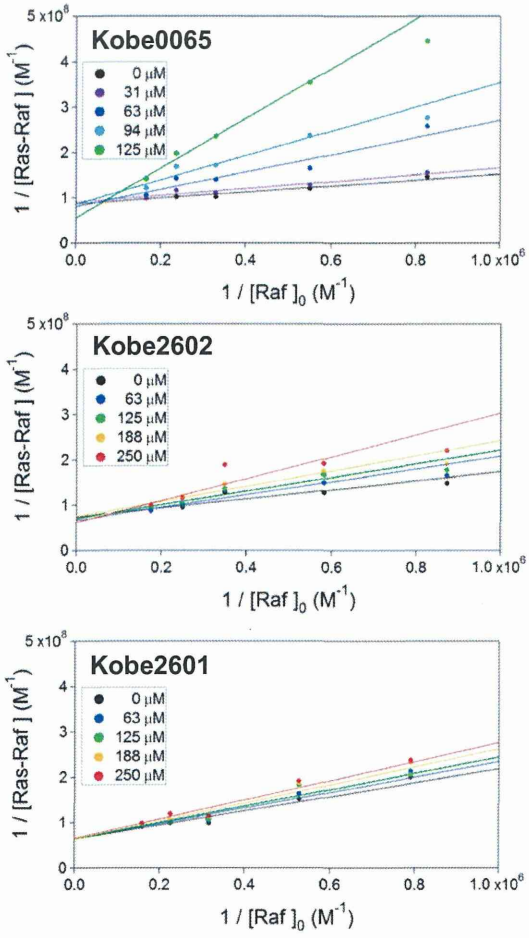

Fig. S1. Kinetic analysis of the inhibition of Ras–Raf binding by the Kobe65-family compounds. H-Ras(1–166) (0.014 μM), preloaded with [γ-^{35}S]GTPγS (1,300–1,800 cpm/pmol), was incubated with varying concentrations of GST-c-Raf-1-RBD (50–131) (0.97–6.31 μM) at 25 °C for 30 min in the presence of the indicated concentrations of the compounds in binding buffer [50 mM Tris·HCl (pH 7.4), 150 mM NaCl, 5 mM $MgCl_2$, 1 mM EDTA, 0.5 mM DTT, 20% DMSO, and 0.01% Triton X-100]. The amount of bound H-Ras was quantified as the radioactivity pulled down by glutathione-sepharose resin. The double reciprocal plots of the concentrations of H-Ras bound to c-Raf-1 RBD ([Ras–Raf]) versus the initial concentrations of c-Raf-1 RBD ($[Raf]_0$) show that the lines obtained for different compound concentrations almost converge on the vertical axis, indicating that the compound exerts competitive inhibition against c-Raf-1 RBD. To obtain K_i values (k_{-1}/k_1) for the compounds, individual datasets were globally fitted according to a scheme of competitive inhibition as follows:

$$Ras{\cdot}Comp + Raf \underset{k_1}{\overset{k_{-1}}{\rightleftarrows}} Ras + Raf + Comp \underset{k_{-2}}{\overset{k_2}{\rightleftarrows}} Ras{\cdot}Raf + Comp,$$

where K_d (k_{-2}/k_2) is a dissociation constant for c-Raf-1 RBD. This reaction can be formulated by the following equation:

$$\frac{1}{[Ras{\cdot}Raf]} = \frac{1}{[Ras]_0} + \frac{K_d}{[Ras]_0[Raf]}\left(1 + \frac{[Comp]}{K_i}\right),$$

where $[Ras]_0$ and $[Comp]$ are the initial concentration of H-Ras·GTPγS and the compounds, respectively. The K_d value for c-Raf-1 RBD was 1.81 ± 1.19 μM and the K_i values for Kobe0065, Kobe2602, and Kobe2601 were 46 ± 13, 149 ± 55, and 773 ± 49 μM, respectively, as calculated from three independent experiments.

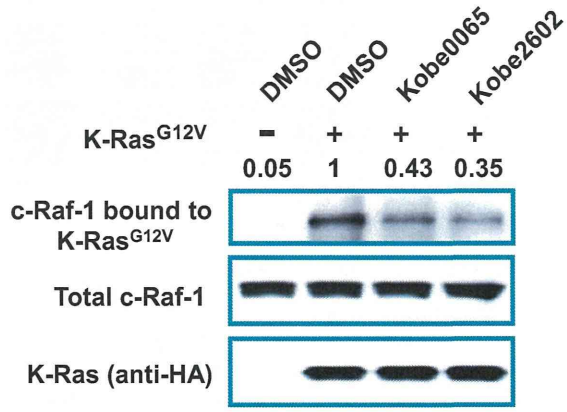

Fig. S2. Inhibition of the K-Ras^{G12V}-c-Raf-1 binding in cells by the Kobe0065-family compounds. NIH 3T3 cells were transfected with pEF-BOS-HA-K-Ras^{G12V} or an empty vector and treated with 20 μM Kobe0065, 20 μM Kobe2602, or the vehicle (DMSO) in the presence of 2% (vol/vol) FBS for 1 h. Cell lysate was subjected to detection of c-Raf-1 coimmunoprecipitated with K-Ras^{G12V} by an anti-HA antibody (*Top*) and total c-Raf-1 (*Middle*) by Western blotting with an anti-c-Raf-1 antibody. The numbers above the lanes show the values of K-Ras-bound/total c-Raf-1 relative to that of the vehicle-treated cells.

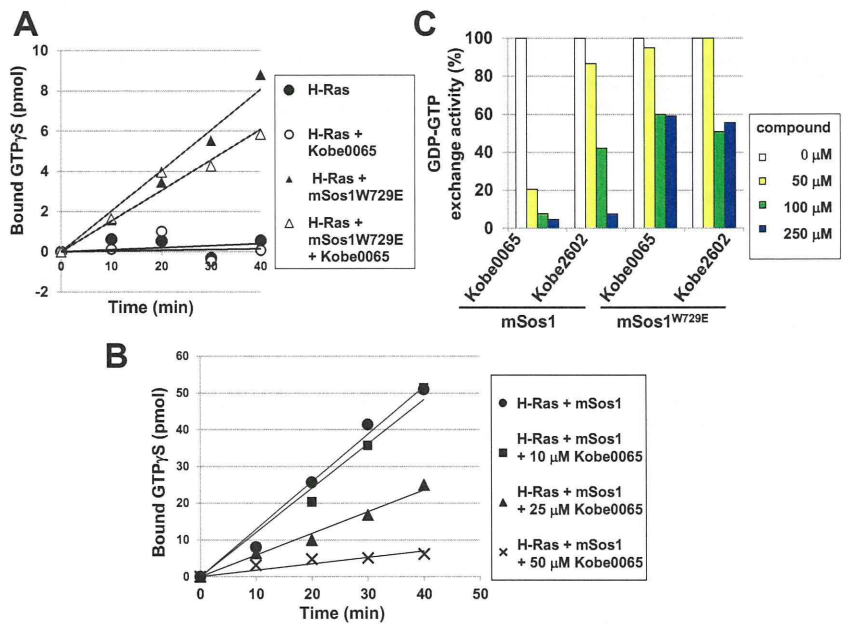

Fig. S3. Effect of the Kobe0065-family compounds on the Sos-stimulated GDP–GTP exchange. (*A*) Effect of Kobe0065 on the mSos1^{W729E}-stimulated nucleotide exchange. The GDP–GTP exchange activity of H-Ras dependent on mSos1^{W729E} was measured as described in the legend to Fig. 2*A* and compared with the intrinsic nucleotide-exchange activity of H-Ras. Three independent experiments yielded essentially equivalent results. (*B*) Dose-dependent inhibition of the mSos1-stimulated nucleotide exchange reaction by Kobe0065. The GDP–GTP exchange activity of H-Ras dependent on mSos1 was measured in the presence of the indicated concentrations of Kobe0065 as described above. (*C*) Dose-dependent inhibition of Sos-stimulated nucleotide exchange by the compounds. The nucleotide exchange activity of H-Ras dependent on mSos1 or mSos1W729E was measured in the presence of the indicated concentrations of the compounds as described above.

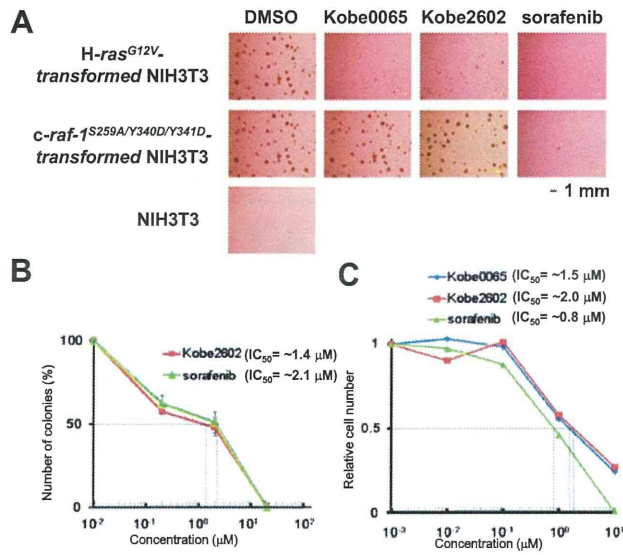

Fig. S4. Specific inhibition of anchorage-independent and -dependent growth of H-*ras*^{G12V}–transformed cells by the Kobe0065-family compounds. (*A*) Effects of the 20 μM compounds on soft agar colony formation of NIH 3T3 cells transformed by the H-*ras*^{G12V} and c-*raf-1*$^{S259A/Y340D/Y341D}$ genes were examined as described in the legend to Fig. 3, *A* and *C*. A representative image is shown for each group. (*B*) The IC_{50} values for Kobe2602 and sorafenib on anchorage-independent growth were estimated from the corresponding dose–response curves. The values are presented as the mean ± SEM; n = 5–6. (*C*) The IC_{50} values for Kobe0065, Kobe2602, and sorafenib on anchorage-dependent growth were estimated from the corresponding dose–response curves. Each point represents the viable cell number at 72 h of treatment relative to the initial number. Shown are representative data.

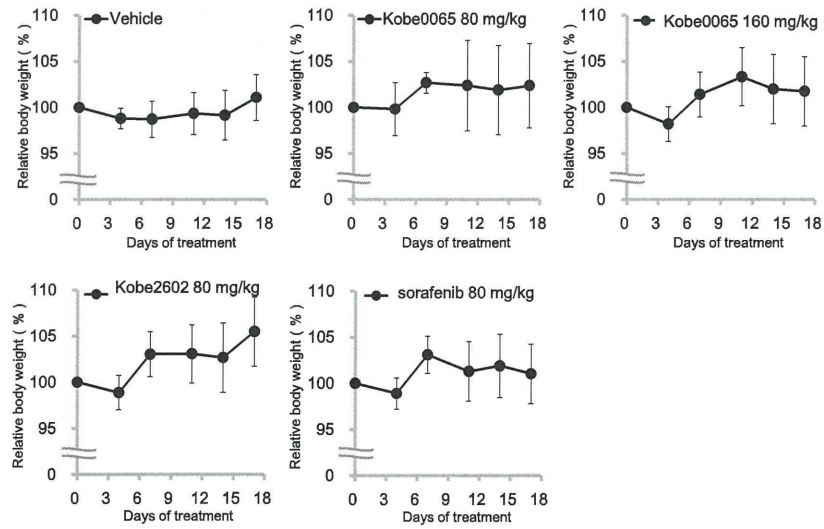

Fig. S5. No significant effect of the administration of the Kobe0065-family compounds on the mouse body weight. The body weight changes of the tumor-grafted mice, administered orally with the indicated doses of the compounds or the vehicle for 17 d (see the legend to Fig. 4*A* and *SI Materials and Methods*) are shown. Each point represents the mouse body weight, the mean ± SEM; n = 8–10 per group, relative to that at day 0.

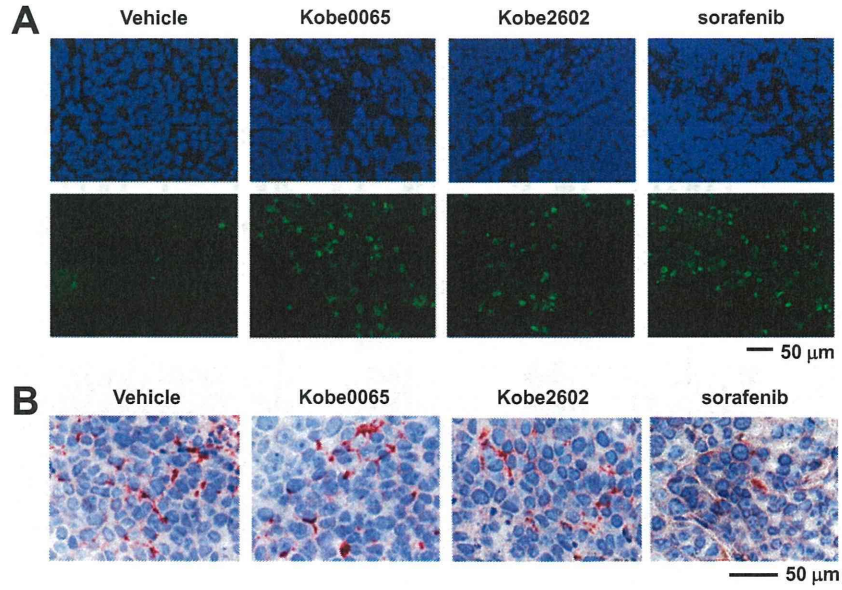

Fig. S6. Effects of the administration of the Kobe0065-family compounds on apoptosis and angiogenesis of tumors. (*A*) Tumors were isolated after daily treatment with the indicated compounds at 80 mg/kg or the vehicle for 17 d and their sections were subjected to staining with DAPI (*Upper*) and the TUNEL assay (*Lower*). (*B*) Tumor sections prepared as described in *A* were subjected to immunohistochemical detection of platelet endothelial cell adhesion molecule-1 with an anti-mouse CD31 antibody (BD Pharmingen). A representative image is shown for each group.

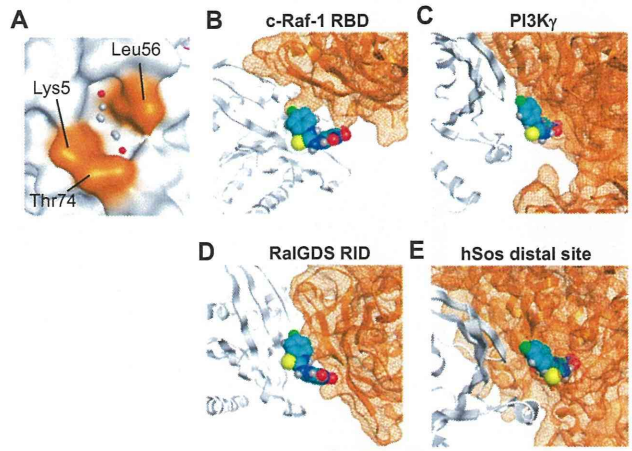

Fig. S7. Structural basis for inhibition of the Ras–effector interactions by the Kobe65-family compounds. (*A*) A close-up view of the Kobe2601-binding pocket in the crystal structure of H-Ras^{T35S}·GppNHp (PDB ID code 3KKM) (1). The cluster of small spheres (hydrophilic, red; hydrophobic, gray) indicates a pocket identified by the Site Finder module in the Molecular Operating Environment (MOE) software package (Chemical Computing Group Inc.). (*B–E*) Predicted spatial configurations of Kobe2601 in various Ras–effector complexes. The NMR structure of the H-Ras^{T35S}·GppNHp–Kobe2601 complex with the lowest energy target function was superimposed on the Ras or Rap1 molecule in the crystal structures of the Rap1A·GppNHp–c-Raf-1 RBD complex (PDB ID code 1C1Y) (*B*), H-Ras^{G12V}·GppNHp–PI3Kγ complex (PDB ID code 1H8E) (*C*), H-Ras^{E31K}·GppNHp–RalGDS RID complex (PDB code ID 1LFD) (*D*), and H-Ras^{Y64A}·GppNHp–hSos complex (PDB ID code 1NVV) (*E*), by fitting to minimize root mean square deviations for the residues 1–31, 39–59, and 76–166, followed by removal of the Ras or Rap1 molecule. H-Ras^{T35S} and the effectors are colored in white and brown, respectively. Kobe2601 is represented by a space-filling model. The fitting and molecular visualization were carried out using the MOE software package.

1. Shima F, et al. (2010) Structural basis for conformational dynamics of GTP-bound Ras protein. *J Biol Chem* 285(29):22696–22705.

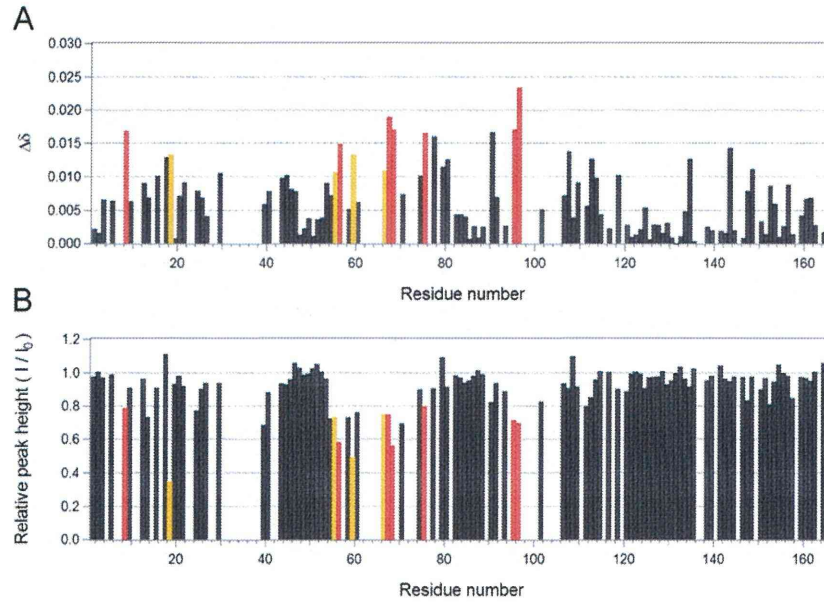

Fig. S8. Mapping of the residues of wild-type H-Ras·GppNHp involved in compound interaction by ^{1}H–^{15}N HSQC spectroscopy. (*A*) Plot of the weighted averages of the backbone ^{1}H and ^{15}N chemical shift changes, calculated by using the function: $\Delta\delta = [\ (\Delta\delta_{1H})^{2} + 0.01(\Delta\delta_{15N})^{2}\ ]^{0.5}$ against the residue numbers. Data are missing for three proline residues, some switch region residues whose signals could not be assigned, and some residues whose signals showed overlaps with others. (*B*) Plot of the peak heights in the presence of Kobe2601 against the residue numbers. Each peak height (I) was normalized relative to that in the absence of the compound (I_0). In the case of the residues that exhibit cross-peak splitting (1), averaged $\Delta\delta$ and I/I_0 values are presented. The perturbed residues with $0.01 \leq \Delta\delta < 0.015$ and $I/I_0 \leq 0.8$, orange; $\Delta\delta \geq 0.015$ and $I/I_0 \leq 0.8$, red. The spectrum in the absence or presence of Kobe2601 was acquired with 2,048 complex points covering 10,000 Hz for ^{1}H and 256 complex points covering 4,000 Hz for ^{15}N and analyzed using Sparky (University of California, San Francisco).

1. Araki M, et al. (2011) Solution structure of the state 1 conformer of GTP-bound H-Ras protein and distinct dynamic properties between the state 1 and state 2 conformers. *J Biol Chem* 286(45):39644–39653.

Fig. S9. Sequence comparison of the residues involved in interaction with Kobe2601 in H-Ras. The amino acid sequences of the residues that exhibit NOE contacts with Kobe2601 and form a hydrophobic surface pocket in H-Ras^{T35S}·GppNHp are conserved among various small GTPases of the Ras and Rho families, as highlighted in yellow. Multiple sequence alignments were generated using the program ClastalX (1).

1. Larkin MA, et al. (2007) Clustal W and Clustal X version 2.0. *Bioinformatics* 23(21):2947–2948.

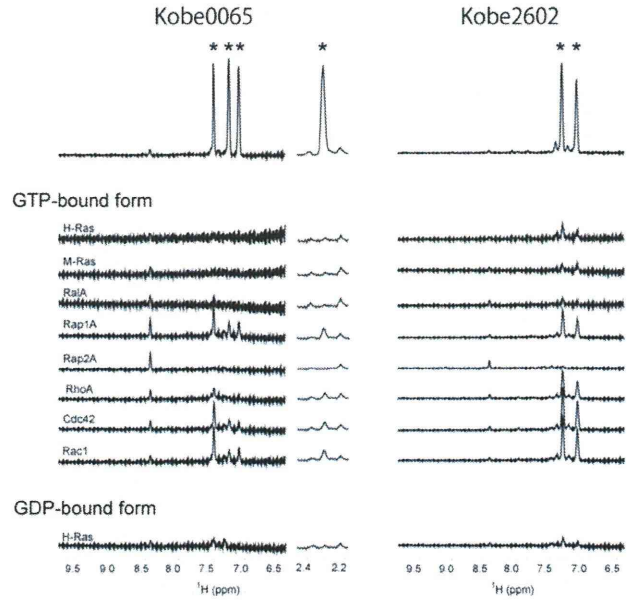

Fig. S10. Relaxation-edited 1D ^{1}H NMR analysis of the interaction of the Kobe0065-family compounds with various small GTPases. Human H-Ras(1–166) and mouse M-Ras(1–178), human RhoA, human Rac1, and human Cdc42 were expressed as GST fusions in *Escherichia coli* using pGEX-6P-1 vector (GE Healthcare), immobilized on glutathione-sepharose resin, and eluted by cleavage with PreScission protease (GE Healthcare) as described previously (1, 2). Human RalA, human Rap1A(1–167), and human Rap2A were expressed with an N-terminal 6xHis tag and affinity-purified as described previously (2). The purified H-Ras was used as the GDP-bound form. Otherwise, the small GTPases were loaded with GppNHp as described previously (2). Direct interaction of Kobe0065 and Kobe2602 with the small GTPases were analyzed at a compound:protein molar ratio of 1:3 by relaxation-edited 1D NMR (3). Kobe2601 could not be used because it underwent a chemical exchange resulting in significant signal attenuation. All of the spectra were acquired with a Carr–Purcell–Meiboom–Gill spin-lock time of 400 ms. The compound-specific signals in the spectra (*Upper*), indicated by asterisks, show line broadening and height reduction and eventually disappear when the compound binds directly to the small GTPases. The residual signal at 8.4 ppm was derived from an impurity in the sample buffer.

1. Shima F, et al. (2010) Structural basis for conformational dynamics of GTP-bound Ras protein. *J Biol Chem* 285(29):22696–22705.
2. Liao J, et al. (2008) Two conformational states of Ras GTPase exhibit differential GTP-binding kinetics. *Biochem Biophys Res Commun* 369(2):327–332.
3. Hajduk PJ, Olejniczak ET, Fesik SW (1997) One-dimensional relaxation- and diffusion-edited NMR methods for screening compounds that bind to macromolecules. *J Am Chem Soc* 119: 12257–12261.

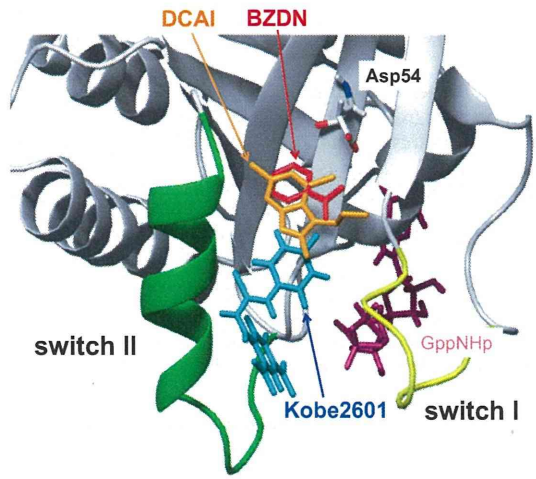

Fig. S11. Comparison of the spatial configurations of Kobe2601 with other Ras inhibitors in the H-Ras^{T35S}·GppNHp structure. The NMR structure of the H-Ras^{T35S}·GppNHp–Kobe2601 complex with the lowest-energy target function was superimposed on K-RasG12D·GTPγS–BZDN (PDB ID code 4DSO) and K-RasG12D·GppCHp–DCAI (PDB ID code 4DST) (1) using the backbone atoms of the residues 1–31, 39–59, and 76–166. The arrangements of benzamidine (BZDN, orange) and 4,6-dichloro-2-methy-3-aminoethyl-indole (DCAI, red) are shown on the backbone structure of the H-Ras^{T35S}·GppNHp–Kobe2601 complex.

1. Maurer T, et al. (2012) Small-molecule ligands bind to a distinct pocket in Ras and inhibit SOS-mediated nucleotide exchange activity. *Proc Natl Acad Sci USA* 109(14):5299–5304.

Table S1. Effect of the Kobe0065-family compounds on the anchorage-independent growth of various human cancer cells

Cell line	Organ	H-Ras	K-Ras	N-Ras	B-Raf	PTEN	PIK3CA	Inhibitory effect, %		
								Kobe0065	Kobe2602	Sorafenib
SW480	Colon		G12V					66.30	65.00	83.80
PANC-1	Pancreas		G12D					63.50	96.00	96.30
EJ-1	Bladder	G12V						62.70	51.50	87.70
HT1080	Tissue			Q61L				79.00	80.50	70.00
DLD-1	Colon		G13D				E545K	60.50	63.00	80.70
HCT116	Colon		G13D				H1047R	55.00	59.00	99.00
A375	Melanoma				V600E			26.00	41.00	93.00
T-47D	Breast						H1047R	11.00	25.00	97.00
LNCap	Prostate					Frameshift		49.00	23.00	87.00
BxPC-3	Pancreas							15.00	24.00	59.70
MCF-7	Breast						E545K	26.00	27.00	93.00
HepG2	Liver							14.50	0	72.50
HeLa	Cervix							13.50	23.50	86.90

Experiments were performed three times, and each experiment used two wells per compound. PIK3CA, phosphatidylinositol-4,5-; PTEN, phosphatase and tensin homolog.

Table S2. Structural statistics for the 15 lowest energy structures of the H-Ras^{T35S}•GppNHp-Kobe2601 complex

Number of distance restraints	
Total	3138
Intramolecular NOEs (H-RasT35S•GppNHp)	
Intraresidue	815
Short-range ($\|i\text{-}j\| = 1$ residue)	749
Medium-range ($\|i\text{-}j\| = 2$ to 4 residues)	532
Long-range ($\|i\text{-}j\| > 4$ residues)	1023
Intermolecular NOEs	19
Number of torsion angle restraints	
ϕ/ψ	114/116
RMSD from experimental restraints	
Distance constraints (Å)	0.0075 ± 0.0009
Torsion angle constraints (°)	0.045 ± 0.029
RMSD from ideal covalent geometry	
Bond lengths (Å)	0.0011 ± 0.0001
Bond angles (°)	0.34 ± 0.01
Impropers (°)	0.29 ± 0.03
RMSD from the mean structure (Å)	
Backbone atoms (residues 1–27, 39–59, 76–166)	0.43 ± 0.06
All heavy atoms (residues 1–27, 39–59, 76–166)	0.83 ± 0.06
Backbone atoms (residues 1–166)	0.78 ± 0.19
All heavy atoms (residues 1–166)	1.21 ± 0.19
Ramachandran analysis	
Most favored regions (%)	82.0
Additional allowed regions (%)	15.5
Generously allowed regions (%)	2.2
Disallowed regions (%)	0.3

Ramachandran analysis was evaluated by the program PROCHECK (1).

1. Laskowski RA, Rullmannn JA, MacArthur MW, Kaptein R, Thornton JM (1996) AQUA and PROCHECK-NMR: programs for checking the quality of protein structures solved by NMR. *J Biomol NMR* 8(4):477–486.

Table S3. NOE upper distance restraints between H-Ras^{T35S}·GppNHp and Kobe2601

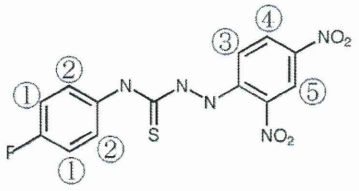

Proton(s) in the protein	Proton(s) in Kobe2601	Upper distance, Å
Lys5 ε	H1	5.0
Lys5 ε	H2	5.4
Leu56 δ1	H1	5.0
Leu56 δ2	H2	5.1
Leu56 δ2	H1	4.9
Met67 ε	H2	4.1
Met67 ε	H3	4.0
Met67 ε	H4	5.2
Met67 ε	H5	3.9
Gln70 γ	H1	5.2
Tyr71 δ	H2	4.4
Tyr71 ε	H1	4.5
Tyr71 ε	H2	5.0
Tyr71 ε	H3	5.1
Thr74 γ2	H1	4.4
Thr74 γ2	H2	4.6
Thr74 γ2	H3	4.5
Thr74 γ2	H4	5.3

Fourteen intermolecular NOEs between methyl or methylene protons in the protein and aromatic protons in the compound were assigned using the ^{13}C-separated NOESY–heteronuclear single quantum coherence spectrum, and four NOEs between aromatic protons from Tyr71 in the protein and aromatic protons in the compound were assigned using the 2D homonuclear NOESY spectra. NOE upper distance restraints were obtained by the CYANA program (1).

1. Güntert P, Mumenthaler C, Wüthrich K (1997) Torsion angle dynamics for NMR structure calculation with the new program DYANA. *J Mol Biol* 273(1):283–298.

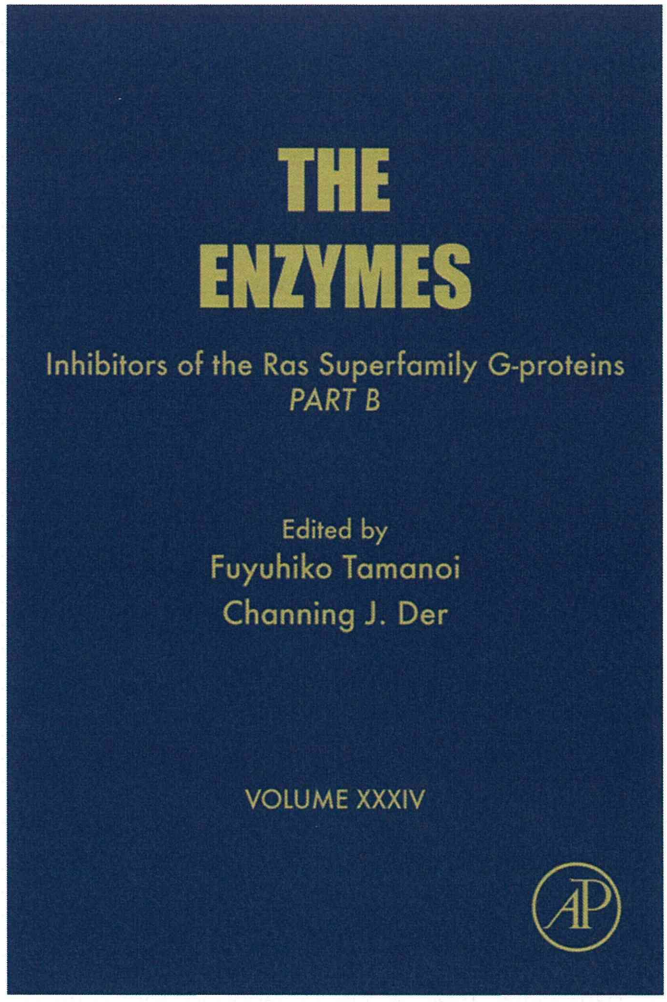

From: Fumi Shima, Yoko Yoshikawa, Shigeyuki Matsumoto, Tohru Kataoka,
Discovery of Small-Molecule Ras Inhibitors that Display Antitumor Activity by Interfering with Ras_GTP–Effector Interaction.
In Fuyuhiko Tamanoi and Channing J. Der, editors: The Enzymes, Vol. 34,
Burlington: Academic Press, 2013, pp. 1-23.
ISBN: 978-0-12-420146-0

CHAPTER ONE

Discovery of Small-Molecule Ras Inhibitors that Display Antitumor Activity by Interfering with Ras·GTP–Effector Interaction

Fumi Shima[1], Yoko Yoshikawa, Shigeyuki Matsumoto, Tohru Kataoka[1]

Division of Molecular Biology, Department of Biochemistry and Molecular Biology, Kobe University Graduate School of Medicine, Kobe, Japan
[1]Corresponding author: e-mail address: kataoka@people.kobe-u.ac.jp

Contents

Abstract

Ras proteins, particularly their active GTP-bound forms (Ras·GTP), were thought "undruggable" owing to the absence of apparent drug-accepting pockets in their crystal structures. Only recently, such pockets have been found in the crystal structures representing a novel Ras·GTP conformation. We have conducted an *in silico* docking screen targeting a pocket in the crystal structure of M-Ras^{P40D}·GTP and obtained Kobe0065, which, along with its analogue Kobe2602, inhibits binding of H-Ras·GTP to c-Raf-1. They inhibit the growth of H-*rasG12V*-transformed NIH3T3 cells, which are accompanied by downregulation of not only MEK/ERK but also Akt, RalA, and Sos, indicating the blockade of interaction with multiple effectors. Moreover, they exhibit antitumor activity on a xenograft of human colon carcinoma carrying *K-rasG12V*. The nuclear magnetic resonance structure of a complex of the compound with H-Ras^{T35S}·GTP confirms its insertion into the surface pocket. Thus, these compounds may serve as a novel scaffold for the development of Ras inhibitors with higher potency and specificity.

The Enzymes, Volume 34
ISSN 1874-6047
http://dx.doi.org/10.1016/B978-0-12-420146-0.00001-9